Second Thresholds in BEC-BCS-Laser Crossover of Exciton-Polariton Systems

Makoto Yamaguchi,[1,*] Kenji Kamide,[1] Ryota Nii,[1] Tetsuo Ogawa,[1,2] and Yoshihisa Yamamoto[3,4]

[1]*Department of Physics, Osaka University, 1-1 Machikaneyama, Toyonaka, Osaka 560-0043, Japan*
[2]*Photon Pioneers Center, Osaka University, 2-1 Yamada-oka, Suita, Osaka 565-0871, Japan*
[3]*National Institute of Informatics, 2-1-2 Hitotsubashi, Chiyoda-ku, Tokyo 101-8403, Japan*
[4]*E. L. Ginzton Laboratory, Stanford University, Stanford, California 94305, USA*

(Dated: April 5, 2013)

The mechanism of second thresholds observed in several experiments is theoretically revealed by studying the BEC-BCS-laser crossover in exciton-polariton systems. We found that there are two different types for the second thresholds; one is a crossover within quasi-equilibrium phases and the other is into non-equilibrium (lasing). In both cases, the light-induced band renormalization causes gaps in the conduction and valence bands, which indicates the exsistence of bound electron-hole pairs in contrast to earlier expectations. We also show that these two types can be distinguished by the gain spectra.

PACS numbers: 71.36.+c, 71.35.Lk, 73.21.-b, 03.75.Gg

In semiconductor exciton-polariton systems, Bose-Einstein condensation (BEC) of exciton-polaritons has been observed in recent years [1–5]. A hot issue is, now, how the exciton-polariton BEC, a thermal equilibrium phenomenon, changes into the lasing operation resulting from the electron-hole (e-h) plasma gain [6], which is essentially a non-equilibrium phenomenon [7, 8]. Earlier experiments show that there are two distinct thresholds when increasing the excitation density: the first threshold is the critical density for the BEC [9, 10] and the second one is recognized as the standard lasing [9–14]. In most cases, the second-threshold mechanism is explained by a shift into the weak coupling regime due to dissociations of bound e-h pairs into the e-h plasma. However, there is no convincing discussion why such dissociations lead to non-equilibriation of the system essential for lasing. As another possibility, a new ordered state involving Bardeen-Cooper-Schrieffer (BCS) -like correlation is also speculated [15]. The second threshold is, thus, currently subject to intense debate. In this letter, our purpose is to reveal the mechanism of the second threshold by studying the BEC-BCS-laser crossover theories [16–18]. As a result, we found that there are two different types for the second threshold; one is a crossover into photonic polariton BEC (quasi-equilibrium phase) [19, 20] and the other is into lasing (non-equilibrium). In both cases, the light-induced band renormalization causes gaps inside the conduction and valence bands, which indicates that there are still light-induced e-h pairs even after the second thresholds, in contrast to the above scenario. We also show that these two types can be distinguished by the gain spectra.

Our starting Hamiltonian is $\hat{H} = \hat{H}_{\rm S} + \hat{H}_{\rm R} + \hat{H}_{\rm SR}$, where

$$\hat{H}_{\rm S} = \hbar\sum_{\alpha,\boldsymbol{k}}\xi_{\alpha,\boldsymbol{k}}\hat{c}^\dagger_{\alpha,\boldsymbol{k}}\hat{c}_{\alpha,\boldsymbol{k}} + \hbar\sum_{\boldsymbol{q}}\xi_{{\rm ph},\boldsymbol{q}}\hat{a}^\dagger_{\boldsymbol{q}}\hat{a}_{\boldsymbol{q}} + \frac{1}{2}\sum_{\boldsymbol{k},\boldsymbol{k}',\boldsymbol{q}}\sum_{\alpha,\alpha'}U'_{\boldsymbol{q}}\hat{c}^\dagger_{\alpha,\boldsymbol{k}+\boldsymbol{q}}\hat{c}^\dagger_{\alpha',\boldsymbol{k}'-\boldsymbol{q}}\hat{c}_{\alpha',\boldsymbol{k}'}\hat{c}_{\alpha,\boldsymbol{k}} - \hbar\sum_{\boldsymbol{k},\boldsymbol{q}}(g^*\hat{a}_{\boldsymbol{q}}\hat{c}^\dagger_{{\rm c},\boldsymbol{k}+\boldsymbol{q}}\hat{c}_{{\rm v},\boldsymbol{k}} + {\rm H.c.}), \quad (1)$$

$$\hat{H}_{\rm R} = \hbar\sum_{\alpha,\boldsymbol{k}}\xi^{\rm B}_{\alpha,\boldsymbol{k}}\hat{b}^\dagger_{\alpha,\boldsymbol{k}}\hat{b}_{\alpha,\boldsymbol{k}} + \hbar\sum_{\boldsymbol{p}}\xi^{\rm B}_{\boldsymbol{p}}\hat{\Psi}^\dagger_{\boldsymbol{p}}\hat{\Psi}_{\boldsymbol{p}}, \quad (2)$$

$$\hat{H}_{\rm SR} = \hbar\sum_{\alpha,\boldsymbol{k},\boldsymbol{q}}\Gamma^\alpha_{\boldsymbol{k}}\hat{c}^\dagger_{\alpha,\boldsymbol{k}}\hat{b}_{\alpha,\boldsymbol{q}} + \hbar\sum_{\boldsymbol{p},\boldsymbol{q}}\zeta_{\boldsymbol{q}}\hat{a}^\dagger_{\boldsymbol{q}}\hat{\Psi}_{\boldsymbol{p}} + {\rm H.c.}, \quad (3)$$

are the system, reservoir, and their interaction Hamiltonians, respectively [18]. Here, $\alpha,\alpha' \in \{{\rm c},{\rm v}\}$, H.c. is the hermitian conjugate, $\hat{c}_{{\rm c},\boldsymbol{k}}$ ($\hat{c}_{{\rm v},\boldsymbol{k}}$) is the conduction (valence) band electron annihilation operators with wavenumber $\boldsymbol{k}$, $U'_{\boldsymbol{q}}$ is the Coulomb interaction, g is the light-matter coupling constant, $\xi_{{\rm c/v},\boldsymbol{k}} \equiv \omega_{{\rm c/v},\boldsymbol{k}} \mp \hbar^{-1}\mu/2$ is the electronic dispersion measured from $\pm\hbar^{-1}\mu/2$, $\hat{a}_{\boldsymbol{q}}$ is the cavity photon annihilation operator with wavenumber $\boldsymbol{q}$, $\xi_{{\rm ph},\boldsymbol{q}} \equiv \omega_{{\rm ph},\boldsymbol{q}} - \hbar^{-1}\mu$ is the photonic dispersion measured from $\hbar^{-1}\mu$, and $\hbar^{-1}\mu$ is an oscillation frequency of the photon and polarization fields, which corresponds to the energy of the main peak in photoluminescence. Similarly, $\hat{b}_{{\rm c},\boldsymbol{k}}$ and $\hat{b}_{{\rm v},\boldsymbol{k}}$ denote fermion annihilation operators of pumping baths and $\hat{\Psi}_{\boldsymbol{p}}$ is a boson annihilation operator of free-space vacuum fields. In this model, Eqs. (2) and (3) are responsible for the incoherent fermionic pumping and photon decay. Based on the above Hamiltonians, we focus on steady states described by the polarization function $p_{\boldsymbol{k}} \equiv \langle\hat{c}^\dagger_{{\rm v},\boldsymbol{k}}\hat{c}_{{\rm c},\boldsymbol{k}}\rangle$, the number of electrons $n_{{\rm e},\boldsymbol{k}} \equiv \langle\hat{c}^\dagger_{{\rm c},\boldsymbol{k}}\hat{c}_{{\rm c},\boldsymbol{k}}\rangle$ and holes $n_{{\rm h},-\boldsymbol{k}} \equiv 1-\langle\hat{c}^\dagger_{{\rm v},\boldsymbol{k}}\hat{c}_{{\rm v},\boldsymbol{k}}\rangle$, and a coherent photon field formed in the $\boldsymbol{q}=0$ state $\langle\hat{a}_{\boldsymbol{q}}\rangle = \delta_{\boldsymbol{q},0}a_0$ with the oscillation frequency $\hbar^{-1}\mu$. These are the minimum variables for describing the BEC, BCS states, and semiconductor lasers.

The band renormalization of the e-h system can, then, be conveniently studied by the poles of the single-particle spectral function $A_{\alpha\alpha'}(\nu;\boldsymbol{k}) \equiv {\rm i}(G^>_{\alpha\alpha'}(\nu;\boldsymbol{k}) - G^<_{\alpha\alpha'}(\nu;\boldsymbol{k}))$, where ${\rm i}\hbar G^>_{\alpha\alpha'}(tt';\boldsymbol{k}) \equiv \langle\hat{c}_{\alpha,\boldsymbol{k}}(t)\hat{c}^\dagger_{\alpha',\boldsymbol{k}}(t')\rangle$ and $-{\rm i}\hbar G^<_{\alpha\alpha'}(tt';\boldsymbol{k}) \equiv \langle\hat{c}^\dagger_{\alpha',\boldsymbol{k}}(t')\hat{c}_{\alpha,\boldsymbol{k}}(t)\rangle$ are the greater and lesser Green's functions in the time domain, respectively.

Within the Hartree-Fock (HF) approximation, a standard Green's function technique yields

$$A_{\rm cv}(\nu;\boldsymbol{k}) = 2u^*_{\boldsymbol{k}}v_{\boldsymbol{k}}[L(\nu,E_{\boldsymbol{k}}) - L(\nu,-E_{\boldsymbol{k}})], \quad (4)$$

$$A_{\rm cc/vv}(\nu;\boldsymbol{k}) = 2|u_{\boldsymbol{k}}|^2 L(\nu,\mp E_{\boldsymbol{k}}) + 2|v_{\boldsymbol{k}}|^2 L(\nu,\pm E_{\boldsymbol{k}}), \quad (5)$$

where $\sqrt{2}u_{\boldsymbol{k}} \equiv [1+\tilde{\xi}^+_{{\rm eh},\boldsymbol{k}}/E_{\boldsymbol{k}}]^{1/2}$ and $\sqrt{2}v_{\boldsymbol{k}} \equiv e^{{\rm i}\theta_{\boldsymbol{k}}}[1-\tilde{\xi}^+_{{\rm eh},\boldsymbol{k}}/E_{\boldsymbol{k}}]^{1/2}$ with $E_{\boldsymbol{k}} \equiv [(\tilde{\xi}^+_{{\rm eh},\boldsymbol{k}})^2 + |\Delta_{\boldsymbol{k}}|^2]^{1/2}$ are the Bogoliubov coefficients, $L(\nu,\pm E_{\boldsymbol{k}}) \equiv \hbar\gamma/[(\hbar\nu - \hbar\tilde{\xi}^-_{{\rm eh},\boldsymbol{k}} \pm \hbar E_{\boldsymbol{k}})^2 + (\hbar\gamma)^2]$ is the Lorentz function, and γ is the thermalization rate of the e-h system [21]. Here, $\tilde{\xi}_{{\rm e/h},\boldsymbol{k}} \equiv \omega_{{\rm e/h},\boldsymbol{k}} + \Sigma^{\rm BGR}_{{\rm e/h},\boldsymbol{k}} - \hbar^{-1}\mu/2$ with $\tilde{\xi}^{\pm}_{{\rm eh},\boldsymbol{k}} \equiv (\tilde{\xi}_{{\rm e},\boldsymbol{k}} \pm \tilde{\xi}_{{\rm h},\boldsymbol{k}})/2$ describes the single particle energy renormalized by the Coulomb interactions $\hbar\Sigma^{\rm BGR}_{{\rm e/h},\boldsymbol{k}} \equiv -\sum_{\boldsymbol{k}'} U'_{\boldsymbol{k}'-\boldsymbol{k}} n_{{\rm e/h},\boldsymbol{k}'}$ and $\Delta_{\boldsymbol{k}}$ is a composite order parameter defined as $\Delta_{\boldsymbol{k}} = |\Delta_{\boldsymbol{k}}|e^{{\rm i}\theta_{\boldsymbol{k}}} \equiv g^* a_0 + \hbar^{-1}\sum_{\boldsymbol{k}'} U'_{\boldsymbol{k}'-\boldsymbol{k}} p_{\boldsymbol{k}'}$. We note that, in the derivation, the notation is transformed into the e-h picture by $\omega_{{\rm e},\boldsymbol{k}} \equiv \omega_{{\rm c},\boldsymbol{k}}$ and $\omega_{{\rm h},\boldsymbol{k}} \equiv -\omega_{{\rm v},\boldsymbol{k}} + \hbar^{-1}\sum_{\boldsymbol{k}'} U'_{\boldsymbol{k}'-\boldsymbol{k}}$.

In Eqs. (4) and (5), there are remarkable similarities to superconductivities [22]. This is because the HF approximation is essentially the same as the mean-field approximation for the system Hamiltonian (Eq. (1)), which can be diagonalized by the Bogoliubov transformations. It is then clear that $\min[2\hbar E_{\boldsymbol{k}}]$ represents the gap energy opened at $\mu/2$ in the renormalized conduction and valence bands (typically Fig. 1 (a) and (b)). Such a picture is well-known for e.g. the BEC-BCS crossover physics but, now, one should notice that Eqs. (4) and (5) are also applicable for *lasing* because thermal equilibrium is not required for their derivations. In the case of lasing, μ is not the chemical potential but the laser frequency and the gap is opened whenever lasing because $a_0 \neq 0$ and $p_{\boldsymbol{k}} \neq 0$ result in $\min[2\hbar E_{\boldsymbol{k}}] \neq 0$. The origin of the gap is analogous to the Rabi splitting in resonance fluorescence [23–25]. This can be understood from the expression of $\min[2\hbar E_{\boldsymbol{k}}] = 2\hbar|g|\sqrt{n_{\rm ph}}$ ($n_{\rm ph} \equiv |a_0|^2$) obtained by assuming free electrons ($U'_{\boldsymbol{q}} = 0$) with $\mu > E_{\rm g}$ ($E_{\rm g}$; the bare band gap energy), which is equivalent to the Rabi frequency in resonance fluorescence. Furethermore, the existence of the gap indicates that light-induced e-h pairs do exist whenever lasing even though there is no e-h pair before lasing. This is one of our important results despite the quite simple analysis. For later convenience, two typical situations for large and small gap energies are shown in Fig. 1 (a) and (b), respectively. In Fig. 1 (a), the renormalized conduction band has a gap around $k \approx 0$ with flattened dispersions because e-h band mixing occurs for large k-regions. In contrast, in Fig. 1 (b), the renormalization is mainly focused on particular k-regions. In both cases, the renormalized bands have gaps at $\mu/2$ and the same holds for the valence band (not shown).

In order to discuss the second-threshold mechanism, however, the unknown variables $\Delta_{\boldsymbol{k}}$ (a_0 and $p_{\boldsymbol{k}}$), $n_{{\rm e},\boldsymbol{k}}$, $n_{{\rm h},\boldsymbol{k}}$, and μ in Eqs. (4) and (5) should be determined in a comprehensive way including BEC, BCS and laser

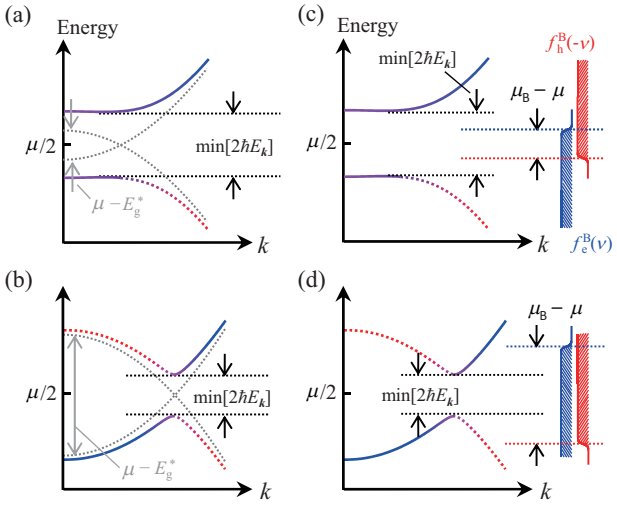

FIG. 1: Renormalized conduction bands for (a) large ($|\mu - E^*_{\rm g}| \lesssim \min[2\hbar E_{\boldsymbol{k}}]$) and (b) small ($\min[2\hbar E_{\boldsymbol{k}}] \lesssim \mu - E^*_{\rm g}$) gap energies. Here, $E^*_{\rm g} \equiv E_{\rm g} + \hbar\Sigma^{\rm BGR}_{{\rm e},\boldsymbol{k}=0} + \hbar\Sigma^{\rm BGR}_{{\rm h},\boldsymbol{k}=0}$ and the gray dashed lines show the energies by ignoring $\Delta_{\boldsymbol{k}}$ in $E_{\boldsymbol{k}}$. Relations to $f^{\rm B}_{\rm e/h}(\pm\nu)$ are also illustrated in panel (c) for quasi-equilibrium ($\min[2\hbar E_{\boldsymbol{k}}] \gtrsim \mu_{\rm B} - \mu + 2\hbar\gamma + 2k_{\rm B}T$) and panel (d) for lasing ($\mu_{\rm B} - \mu \gtrsim \min[2\hbar E_{\boldsymbol{k}}] + 2\hbar\gamma + 2k_{\rm B}T$). $\omega_{{\rm e},k} = \omega_{{\rm h},k}$ and $\mu^{\rm B}_{\rm e} = \mu^{\rm B}_{\rm h}$ are assumed.

physics [16–18]. Within the HF approximation, the simultaneous equations can be written as

$$\hbar\Delta_{\boldsymbol{k}} = \sum_{\boldsymbol{k}'} U^{{\rm eff},\kappa}_{\boldsymbol{k}',\boldsymbol{k}} \int_{-\infty}^{\infty} \frac{{\rm d}[\hbar\nu]}{2\pi} f^{\rm NESS}_{{\rm eh},\boldsymbol{k}'}(\nu) A_{\rm cv}(\nu;\boldsymbol{k}'), \quad (6)$$

$$n_{{\rm e/h},\boldsymbol{k}} = \int_{-\infty}^{\infty} \frac{{\rm d}[\hbar\nu]}{2\pi} f^{\rm NESS}_{{\rm e/h},\boldsymbol{k}}(\nu) A_{\rm cc/vv}(\pm\nu;\boldsymbol{k}), \quad (7)$$

where $U^{{\rm eff},\kappa}_{\boldsymbol{k}',\boldsymbol{k}} \equiv \hbar|g|^2/(\xi_{{\rm ph},0} - {\rm i}\kappa) + U'_{\boldsymbol{k}'-\boldsymbol{k}}$ is the effective e-h attraction and κ is the photon loss rate [21]. Eaxt expressions of $f^{\rm NESS}_{{\rm eh},\boldsymbol{k}}(\nu)$ and $f^{\rm NESS}_{{\rm e/h},\boldsymbol{k}}(\nu)$ are given in supplementary [21], which are described by the bath Fermi distribution functions $f^{\rm B}_{\rm e/h}(\nu) \equiv [\exp(\beta(\hbar\nu - (\mu^{\rm B}_{\rm e/h} - \mu/2))) + 1]^{-1}$ with the inverse temperature $\beta \equiv 1/k_{\rm B}T$ and the chemical potentials $\mu^{\rm B}_{\rm e/h}$. The important point here is that, by assuming $\omega_{{\rm e},\boldsymbol{k}} = \omega_{{\rm h},\boldsymbol{k}}$ and a charge neutrality $\mu^{\rm B}_{\rm e} = \mu^{\rm B}_{\rm h}$ with $\mu_{\rm B} \equiv \mu^{\rm B}_{\rm e} + \mu^{\rm B}_{\rm h}$, Eqs. (6) and (7) can recover the BCS gap equation when (I) $\min[2\hbar E_{\boldsymbol{k}}] \gtrsim \mu_{\rm B} - \mu + 2\hbar\gamma + 2k_{\rm B}T$ (quasi-equilibrium), while there are k-regions described by the Maxwell-Semiconductor-Bloch equations when (II) $\mu_{\rm B} - \mu \gtrsim \min[2\hbar E_{\boldsymbol{k}}] + 2\hbar\gamma + 2k_{\rm B}T$ (lasing states; BCS-coupled lasing in a strict sense). The physical meanings of these conditions are discussed in detail in Ref. [18] and not repeated here. Instead, these conditions are illustrated in Fig. 1 (c) and (d) in relation to $f^{\rm B}_{\rm e/h}(\pm\nu)$ for quasi-equilibrium and lasing conditions, respectively. It is, then, clear that the system enters into lasing phases when $\mu_{\rm B} - \mu$ roughly goes beyond the energy gap of $\min[2\hbar E_{\boldsymbol{k}}]$ by ignoring the broadening due to γ and T.

Based on the above formalism, we have performed numerical calculations, where the cavity level ($= \hbar\omega_{{\rm ph},0}$)

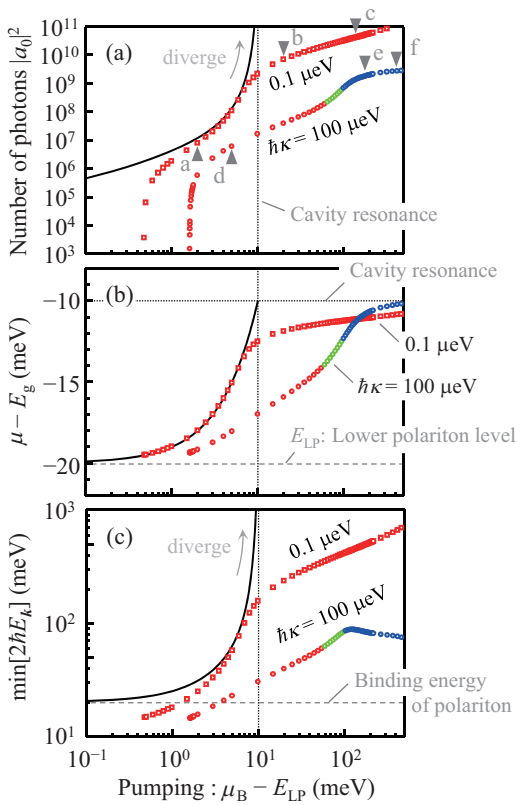

FIG. 2: Numerical solutions of (a) the number of photons $|a_0|^2$, (b) the oscillation frequency μ, and (c) the gap energy $\min[2\hbar E_{\boldsymbol{k}}]$ as a function μ_B for $\hbar\kappa = 0.1$ μeV and 100 μeV. Red and blue colors are used when satisfying the condition (I) for quasi-equilibrium and the condition (II) for lasing in the text, respectively. Green colors are used when both of them are not satisfied. For comparison, black solid lines show the results by thermal-equilibrium theories [19, 20].

is in resonance with the (1S) exciton level located at 10 meV below E_g and the lower polariton level E_{LP} is formed at 20 meV below E_g [21]. For $\hbar\kappa$, we have used values of 0.1 μeV and 100 μeV to study the effects of non-equilibrium. We note, however, that $\hbar\kappa = 100$ μeV is a reasonable value in current experiments. Fig. 2 shows the calculated results of $|a_0|^2$, μ, and $\min[2\hbar E_{\boldsymbol{k}}]$ as a function of μ_B, the pumping parameter. In the case of the equilibrium theories, $|a_0|^2$ diverges in the limit of $\mu_B \to \hbar\omega_{ph,0}$ because it is preferable to increase photons rather than electrons and holes due to the phase space filling effects. As a result, the photonic polariton BEC is achieved by the photon-mediated e-h attraction [19, 20]. In contrast, in the case with finite pumping and losses (plots), the behaviors are different in many aspects. Focusing on the plots for $\hbar\kappa = 0.1$ μeV, two distinct thresholds can be seen ($\mu_B - E_{LP} \approx 5.0 \times 10^{-1}$ meV and 6.0×10^{0} meV) in Fig. 2 (a). At the same time, μ is gradually blue-shifted from E_{LP} and then approaches the bare cavity resonance. Similar qualitative behavior also can be seen for $\hbar\kappa = 100$ μeV. These behaviors are consistent with experiments. However, there is a crucial difference be-

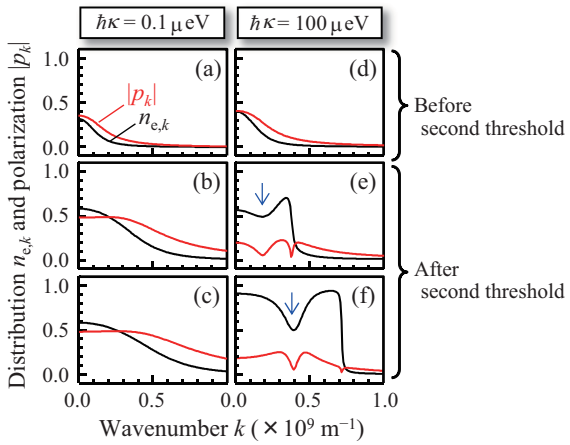

FIG. 3: Calculated distributions $n_{e,k}$ and polarizations $|p_k|$ corresponding to the triangles indicated by a-f in Fig. 2 (a). Panel (a)-(c) are for $\hbar\kappa = 0.1$ μeV and panel (d)-(f) are for $\hbar\kappa = 100$ μeV. Arrows show the kinetic hole burning.

tween the two; according to the above-mentioned conditions (I) and (II), all plots are in quasi-equilibrium for $\hbar\kappa = 0.1$ μeV but there are plots (blue) in lasing for $\hbar\kappa = 100$ μeV after the second threshold.

The difference is also reflected in $n_{e,k}$ and p_k, as shown in Fig. 3. Before the second thresholds, $n_{e,k}$ and p_k for $\hbar\kappa = 0.1$ μeV (Fig. 3 (a)) are similar to those for $\hbar\kappa = 100$ μeV (Fig. 3 (d)). However, after the second thresholds, $n_{e,k}$ and p_k are quite different, depending on the value of $\hbar\kappa$. In the case of $\hbar\kappa = 0.1$ μeV, $n_{e,k}$ monotonically decreases as a function of k and p_k has a plateau ≈ 0.5 (Fig. 3 (b) and (c)), which are the same features as the photonic polariton BEC in thermal equilibrium [19, 20]. In contrast, in the case of $\hbar\kappa = 100$ μeV, the kinetic hole burning appears as a signature of lasing and the Fermi surface is formed with the population inversion $n_{e,k} > 0.5$ (Fig. 3 (e)). For larger μ_B, such behaviors become much more pronounced (Fig. 3 (f)). These results directly show that the second thresholds for $\hbar\kappa = 0.1$ μeV and 100 μeV in Fig. 2 (a) are formed by different mechanisms.

In fact, for $\hbar\kappa = 0.1$ μeV, the second threshold is formed by the same mechanism as the photon divergence in the equilibrium theories, and therefore, it results from the crossover into the photonic polariton BEC. In the present case, there are finite losses of cavity photons even if the system is in quasi-equilibrium. As a result, the divergence is avoided and the second threshold appears instead. After the second threshold, the monotonic increase of $\min[2\hbar E_{\boldsymbol{k}}]$ (Fig. 2 (c)) indicates the enhancement of the light-induced e-h paring and expands the flattened region of dispersion in Fig. 1 (a). It is, then, clear that the plateau of $p_k \approx 0.5$ in Fig. 3 (b) and (c) is formed by the e-h mixing around such flattened dispersions. In the case of $\hbar\kappa = 100$ μeV, on the other hand, the second threshold is related to the crossover into lasing, explained as follows. Before the second threshold, the system stays

in quasi-equilibrium (red circles in Fig. 2), where the relationship between the renormalized band and the pumping baths is well expressed in Fig. 1 (c). In this situation, the pumping is blocked inside the gap $\min[2\hbar E_{\boldsymbol{k}}]$. However, by increasing the pumping $\mu_{\rm B}$, $\mu_{\rm B}-\mu$ exceed the gap, $\mu_{\rm B}-\mu \gtrsim \min[2\hbar E_{\boldsymbol{k}}]$, and then, electrons above the gap can be supplied suddenly. Such a feeding mechanism causes a rapid increase of photons, resulting in the second threshold. Here, by ignoring the effects of γ and T, this situation $\mu_{\rm B}-\mu \gtrsim \min[2\hbar E_{\boldsymbol{k}}]$ is equivalent to the above-described condition (II) for the lasing phases. Consequently, the second threshold is accompanied by the change into lasing (non-equilibrium). By increasing the pumping further, μ is fixed around the cavity (Fig. 2 (b)), $\min[2\hbar E_{\boldsymbol{k}}]$ is decreased (Fig. 2 (c)), and the effective band gap $E_{\rm g}^{*} \equiv E_{\rm g}+\hbar\Sigma^{\rm BGR}_{{\rm e},\boldsymbol{k}=0}+\hbar\Sigma^{\rm BGR}_{{\rm h},\boldsymbol{k}=0}$ shrinks, of course. The lasing situation is then well captured in Fig. 1 (d), where the gap $\min[2\hbar E_{\boldsymbol{k}}]$ is decreased but still opened around the laser frequency. The decrease of the gap for $\mu_{\rm B}-\mu \gtrsim \min[2\hbar E_{\boldsymbol{k}}]$ implies that the particle flux $\mu_{\rm B}-\mu$ beyond $\min[2\hbar E_{\boldsymbol{k}}]$ act toward e-h pair breaking but the e-h pairs cannot be fully dissociated because $\min[2\hbar E_{\boldsymbol{k}}] \neq 0$. As a result, light-induced e-h pairs are still formed around the laser frequency, typically around the energy regions of the kinetic hole burning (Fig. 3 (e) and (f)). This is, in turn, somewhat analogous to the e-h Cooper pairs formed around the Fermi energy, i.e. weakly correlated e-h pairs in momentum space. The difference is that the e-h pairs are formed around the laser frequency rather than the Fermi energy.

These results indicate that it would be reasonable to explain the second thresholds reported in current experiments by the crossover into lasing because $\kappa = 100$ μeV is a reasonable value for them, in agreement with earlier explanations [9, 11–14]. Our theory, however, show that the crossover is not accompanied by the dissociations of bound e-h pairs. Instead, the pairing mechanism changes into the light-induced one around the laser frequency. This is in contrast to the commonly accepted ideas but a natural picture of lasing.

We have thus discussed the two different types of the second threshold. However, it is difficult to directly distinguish them by the excitation dependence of the number of photons (Fig. 2 (a)), in principle. Therefore, we finally study the measurable optical gain spectra $G(\omega)$ [26, 27] by assuming an additional perturbative Hamiltonian $\hat{H}'(t) = -F(t)\sum_{\boldsymbol{k}} d_{\rm cv}(\hat{c}^{\dagger}_{{\rm c},\boldsymbol{k}}\hat{c}_{{\rm v},\boldsymbol{k}} + {\rm H.c.})$. Here, $F(t)$ is the weak light field irradiated from the outside and $d_{\rm cv}$ is the dipole matrix element. Within the linear response [28], $G(\omega)$ is estimated with the ladder approximation [29]. Figure 4 (a)-(f) shows the gain spectra corresponding to Fig. 3 (a)-(f), respectively. In the case of $\hbar\kappa = 0.1$ μeV, two absorption peaks can be found, which result from the two flattened dispersions shown in Fig. 1 (a). Therefore, the separation of the peaks corresponds to $\min[4\hbar E_{\boldsymbol{k}}]$, the sum of the gaps in the conduction and valence bands. Here, we note that absorption dominates the spectra because there is no or little population inversion ($n_{{\rm e},k} > 0.5$) for the condensed phases in equilibrium (Fig. 3 (a)-(c)). In the case of $\hbar\kappa = 100$ μeV, however, gain appears when the system enters into the lasing phase (Fig. 4 (e) and (f)) although absorption still dominates in the quasi-equilibrium case (Fig. 4 (d)). The spectral hole (or gap) with a separation of $\min[4\hbar E_{\boldsymbol{k}}]$ in Fig. 4 (f) reflects the gap formed in the renormalized band (Fig. 1 (d)). The existence of the gain after the second threshold is due to the population inversion for lasing (Fig. 3 (e) and (f)) and, as a result, can be used to distinguish the two types of the second threshold in experiments.

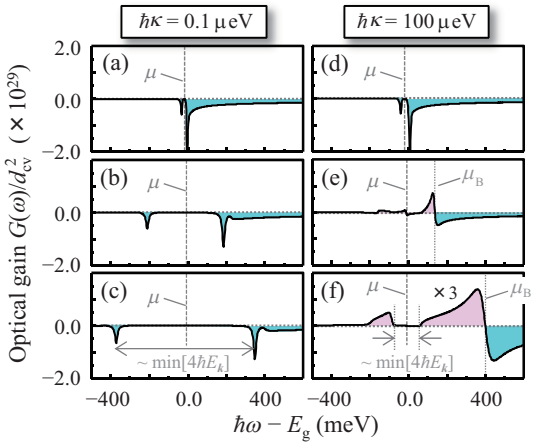

FIG. 4: Optical gain spectra. Panel (a)-(f) corresponds to Fig. 3 (a)-(f), respectively. Positive (red) and negative (blue) values represents the gain and absorption, respectively.

To summarize, we have shown that there are two different types for the second threshold. In both cases, dissociations of bound e-h pairs do not occur due to the light-induced pairing, in contrast to earlier expectations. The gain spectra are also studied and the existence of the gain would be useful to distinguish the two different types of the second threshold.

We are grateful to T. Horikiri, Y. Shikano, M. Bamba, T. Yuge, K. Asano, T. Ohashi, H. Akiyama, M. Kuwata-Gonokami, T. Inagaki, P. Huai, H. Ajiki, J. Keeling and P. B. Littlewood for fruitful discussions. This work is supported by the JSPS through its FIRST Program, and DYCE, KAKENHI 20104008.

* E-mail: yamaguchi@acty.phys.sci.osaka-u.ac.jp

[1] H. Deng, G. Weihs, C. Santori, J. Bloch, Y. Yamamoto, Science **298**, 199 (2002).
[2] J. Kasprzak *et al*, Nature **443**, 409 (2006).
[3] R. Balili *et al*, Science **316**, 1007 (2007).
[4] S. Utsunomiya *et al*, Nature Phys. **4**, 700 (2008).
[5] T. Horikiri *et al*, Phys. Rev. B **81**, 033307 (2010).
[6] W. W. Chow, S. W. Koch, and M. Sergent III, *Semiconductor-Laser Physics*, (Springer-Verlag, Berlin, 1994).

[7] D. Bajoni *et al*, Phys. Rev. Lett. **100**, 047401 (2008).
[8] J. Kasprzak, D. D. Solnyshkov, R. Andre, L. S. Dang, and G. Malpuech, Phys. Rev. Lett. **101**, 146404 (2008).
[9] R. Balili, B. Nelsen, D. W. Snoke, L. Pfeiffer, and K. West, Phys. Rev. B. **79**, 075319 (2009).
[10] B. Nelsen *et al*, J. Appl. Phys. **105**, 122414 (2009).
[11] L. S. Dang, D. Heger, R. Andre, F. Boeuf, and R. Romestain, Phys. Rev. Lett. **81**, 3920 (1998).
[12] J.-S. Tempel *et al*, Phys. Rev. B. **85**, 075318 (2012); New J. Phys. **14**, 083014 (2012).
[13] P. Tsotsis *et al*, New J. Phys. **14**, 023060 (2012).
[14] E. Kamman *et al*, New J. Phys. **14**, 105003 (2012).
[15] H. Deng, H. Haug, and Y. Yamamoto *et al*, Rev. Mod. Phys. **82**, 1489 (2010).
[16] M. H. Szymanska, J. Keeling, and P. B. Littlewood, Phys. Rev. Lett. **96**, 230602 (2006); Phys. Rev. B **75**, 195331 (2007).
[17] J. Keeling, M. H. Szymanska, and P. B. Littlewood, in *Keldysh Green's function's approach to coherence in a non-equilibrium steady state: connecting Bose-Einstein condensation and lasing*, edited by G. Slavcheva and P. Roussignol, Optical Generation and Control of Quantum Coherence in Semiconductor Nanostructures (Springer-Verlag, Berlin, 2010).
[18] M. Yamaguchi, K. Kamide, T. Ogawa, and Y. Yamamoto, New J. Phys. **14**, 065001 (2012).
[19] K. Kamide and T. Ogawa, Phys. Rev. Lett. **105**, 056401 (2010); Phys. Rev. B **83**, 165319 (2011).
[20] T. Byrnes, T. Horikiri, N. Ishida, and Y. Yamamoto, Phys. Rev. Lett. **105**, 186402 (2010).
[21] See Supplemental Material at [URL will be inserted by publisher] for details.
[22] A. A. Abrikosov, L. P. Gorkov, and I. E. Dzyaloshinskii, *Methods of Quantum Field Theory in Statistical Physics*, (Pergamon, New York, 1975).
[23] M. O. Scully and M. S. Zubairy, *Quantum Optics*, (Cambridge University Press, New York, 1977).
[24] S. Schmitt-Rink, D. S. Chemla, and H. Haug, Phys. Rev. B, **37**, 941 (1988).
[25] T. Horikiri *et al*, in preparation.
[26] Y. Takahashi *et al*, Appl. Phys. Lett. **86**, 243101 (2005).
[27] M. Yoshita *et al*, Appl. Phys. Lett. **100**, 112101 (2012).
[28] A. Shimizu and T. Yuge, J. Phys. Soc. Jpn. **79**, 013002 (2010).
[29] H. Haug and S. Schmitt-Rink, Prog. Quantum Electron. **9**, 3 (1984).

Supplemental material

In this supplementary material, we describe a few details of our formalism in order to make the paper self-contained. We also describe the parameters in our numerical calculations and compare the results with our own previous study [Yamaguchi *et al*, New J. Phys. **14**, 065001 (2012)].

A few details of the formalism

In the main text, the thermalization rate and the photon loss rate are described by γ and κ, which result from the system-bath interaction Hamiltonian Eq. (3). With the definitions of the density of states

$$D^{\rm B}_{\alpha}(\omega) \equiv \sum_{\boldsymbol{k}} \delta(\omega^{\rm B}_{\alpha,\boldsymbol{k}} - \omega),\ D^{\rm B}_{\rm ph}(\omega) \equiv \sum_{\boldsymbol{p}} \delta(\omega^{\rm B}_{\boldsymbol{p}} - \omega), \tag{8}$$

γ and κ have the following relations with $\mathit{\Gamma}^{\alpha}_{\boldsymbol{k}}$ and $\zeta_{\boldsymbol{q}}$:

$$\gamma \cong \gamma_{\alpha,\boldsymbol{k}} \cong \pi|\mathit{\Gamma}^{\alpha}_{\boldsymbol{k}}|^2 D^{\rm B}_{\alpha}(\omega),\ \kappa \cong \kappa_{\boldsymbol{q}} \cong \pi|\zeta_{\boldsymbol{q}}|^2 D^{\rm B}_{\rm ph}(\omega). \tag{9}$$

Here, the dependence on the wavenumber is neglected for simplicity.

In addition, in Eqs. (6) and (7), the distributions of $f^{\rm NESS}_{\rm eh,\boldsymbol{k}}(\nu)$ and $f^{\rm NESS}_{\rm e/h,\boldsymbol{k}}(\nu)$ are defined as

$$f^{\rm NESS}_{\rm eh,\boldsymbol{k}}(\nu) \equiv \frac{1}{2}[f^{\rm B}_{\rm e}(\nu) - f^{\rm B}_{\rm h}(-\nu)] + \frac{1}{2}[f^{\rm B}_{\rm e}(\nu) + f^{\rm B}_{\rm h}(-\nu) - 1]\frac{\tilde{\xi}^{+}_{\rm eh,\boldsymbol{k}} + {\rm i}\gamma}{\nu - \tilde{\xi}^{-}_{\rm eh,\boldsymbol{k}}}, \tag{10}$$

$$f^{\rm NESS}_{\rm e/h,\boldsymbol{k}}(\nu) \equiv f^{\rm B}_{\rm e/h}(\nu)\eta_{\rm e/h,\boldsymbol{k}}(\nu) + [1 - f^{\rm B}_{\rm h/e}(-\nu)][1 - \eta_{\rm e/h,\boldsymbol{k}}(\nu)], \tag{11}$$

where $\eta_{\rm e/h,\boldsymbol{k}}(\nu)$ is

$$\eta_{\rm e/h,\boldsymbol{k}}(\nu) \equiv \frac{(\nu + \tilde{\xi}_{\rm h/e,\boldsymbol{k}})^2 + \gamma^2}{(\nu + \tilde{\xi}_{\rm h/e,\boldsymbol{k}})^2 + \gamma^2 + |\mathit{\Delta}_{\boldsymbol{k}}|^2}, \tag{12}$$

with $0 \leq \eta_{\rm e/h,\boldsymbol{k}}(\nu) \leq 1$. Then, from Eqs. (6), (7), (10) and (11), it can be found that the band renormalization effects are included not only in $A_{\alpha\alpha'}(\nu;\boldsymbol{k})$ but also in $f^{\rm NESS}_{\rm e/h,\boldsymbol{k}}(\nu)$. For example, in Eq. (11), $\eta_{\rm e/h,\boldsymbol{k}}(\nu) = 1$ and

$f^{\rm NESS}_{{\rm e/h},\boldsymbol{k}}(\nu) = f^{\rm B}_{\rm e/h}(\nu)$ when $\Delta_{\boldsymbol{k}} = 0$. This means that electrons and holes are thermalized into the simple Fermi distribution. However, there exists e-h band mixing when $\Delta_{\boldsymbol{k}} \neq 0$, and therefore $f^{\rm NESS}_{{\rm e/h},\boldsymbol{k}}(\nu)$ is influenced by $1 - f^{\rm B}_{\rm h/e}(\nu)$ with a weighting factor of $1 - \eta_{{\rm e/h},\boldsymbol{k}}(\nu)$, as seen in Eq. (11).

Parameters in the numerical calculations

In our numerical calculations, the $\boldsymbol{k}$-dependence of $\Delta_{\boldsymbol{k}}$ is eliminated by using a contact potential $U'_{\boldsymbol{q}} = U$ and the other parameters are $\hbar\omega_{{\rm e},\boldsymbol{k}} = \hbar\omega_{{\rm h},\boldsymbol{k}} = \hbar^2k^2/2m + E_{\rm g}/2$, $m = 0.068m_0$ (m_0 is the free electron mass), $\mu^{\rm B}_{\rm e} = \mu^{\rm B}_{\rm h}$, $T =$ 10 K, and $\hbar\gamma = 4$ meV. In this context, we note that the calculations are qualitative even though these parameters are taken as realistic as possible. Here, the contact potential and the coupling constant are, respectively, set as $U = 2.66 \times 10^{-10}$ eV and $\hbar g = 6.29 \times 10^{-7}$ eV with cut-off wavenumber $k_{\rm c} = 1.36 \times 10^9\ m^{-1}$. In this case, the (1S) exciton level ($\equiv E_{\rm ex}$) is formed at 10 meV below $E_{\rm g}$ ($E_{\rm ex} = E_{\rm g} - 10$ meV) and the lower polariton level $E_{\rm LP}$ is created at 20 meV below $E_{\rm g}$ ($E_{\rm LP} = E_{\rm g} - 20$ meV) under the resonant condition $\hbar\omega_{\rm ph,0} = E_{\rm ex}$, as described in the main text.

Comparisons with our previous results

In the present study, there are mainly two differences from the previous conditions of numerical calculations reported in Ref. [S1]. The first difference is the cavity detuning; the cavity resonance $\hbar\omega_{\rm ph,0}$ is tuned to the exciton level $E_{\rm ex}$ in the present case ($\hbar\omega_{\rm ph,0} = E_{\rm ex} = E_{\rm g} - 10$ meV), whereas it is largely detuned from the exciton level in Ref. [S1] ($\hbar\omega_{\rm ph,0} = E_{\rm ex} + 40$ meV $= E_{\rm g} + 30$ meV). The second difference is the value of the coupling constant $\hbar g$ which determines the position of the lower polariton level under the resonant condition; the lower polariton level is located at 10 meV below the exction level in the present case ($E_{\rm LP} = E_{\rm ex} - 10$ meV), while it is at 5 meV below the exciton level in Ref. [S1] ($E_{\rm LP} = E_{\rm ex} - 5$ meV). Based on these differences [S2], we compare the previous and present numerical results here.

In the previous case, as a result of the large detuning and the small coupling constant, the cavity has little influence on the behavior of excitons formed in the low density regime. Only in a high density regime, the cavity has large influence on the behavior of the condensation but excitons no longer exist in the high density regime. Such signatures can be found in Fig. 10 and Fig. 11 of Ref. [S1]. Red and blue plots in Fig. 10 (a) show that the order parameter $\hbar\Delta$ comes up around $\mu_{\rm B} - E_{\rm g} = 10$ meV when $\mu_{\rm B}$ is increased, as indicated by the arrow (A). This means that the condensation starts when $\mu_{\rm B}$ reaches around the exciton level, i.e. $\mu_{\rm B} = E_{\rm ex} = E_{\rm g} - 10$ meV and there is, indeed, little influence of the cavity. In addition, Fig. 11 (A) shows that $n_{{\rm e},k}$ and $|p_k|$ monotonically decrease in the k-space. Therefore, the condensation indicated by (A) in Fig. 10 (a) is identified as the exciton BEC. The negligibly small photonic fraction around the point (A) in Fig. 11 is also consistent with this interpretation. Here, we note that the photonic fraction is still small even though $\mu_{\rm B}$ is increased up to around the point (B). Hence, the effect of the cavity is still small at this point. However, in contrast to Fig. 11 (A), Fig. 11 (B) shows that $n_{{\rm e},k}$ has a rounded shape of the Fermi function and $|p_k|$ has a peak around the Fermi surface. Therefore, the condensation around the point (B) can be classified as the electron-hole (e-h) BCS phase. It should be noted that, at this stage, there is no exciton anymore because the density is increased as much as the Fermi surface is formed. This means that the cavity has little influence on the crossover from the exciton BEC to the e-h BCS phase. In this regime, it is natural that there is little effect of the cavity loss κ in Fig. 10 (a)-(c) (the difference between the red and blue plots for $\mu_{\rm B} \lesssim \hbar\omega_{\rm ph,0}$). This effect becomes apparent only after $\mu_{\rm B}$ is increased up to around the cavity resonance ($\mu_{\rm B} \gtrsim \hbar\omega_{\rm ph,0}$) but excitons no longer exist in this situation, as described above.

In the present case, on the other hand, the cavity has large influence on the condensation even in the low density regime due to the resonance condition and the larger coupling constant. In Fig. 2 (a), it can be found that the condensation occurs when $\mu_{\rm B}$ is around $E_{\rm LP}$ rather than the exciton level. Given the monotonic decrease of $n_{{\rm e},k}$ and $|p_k|$ in k-space, as shown in Fig. 3 (a) and (d), the condensation can be identified as the exciton-polariton BEC. As a result, the cavity loss κ also has a great impact on the behavior of the condensation, as evidenced in Fig. 2 (a)-(c) (the differences between the plots of $\kappa = 0.1$ μeV and $\kappa = 100$ μeV). This is in contrast to the previous results where κ plays no role in the low density regime ($\mu_{\rm B} \lesssim \hbar\omega_{\rm ph,0}$ in Fig. 10 (a)-(c) of Ref. [S1]). However, when $\mu_{\rm B}$ is largely increased, the situation is not so different from the previous calculations. This is because the band gap renormalization decreases the effective band gap $E^*_{\rm g}$ and the cavity level enters into the conduction and valence bands. Therefore, for example, the behaviors of $n_{{\rm e},k}$ and $|p_k|$ after the second thresholds in Fig. 3 are similar to those in Fig. 11 (E) and (H) of Ref. [S1]. Thus, from the comparison of the present and previous numerical results, we can

learn that the effect of the cavity in the low density regime becomes more important in the present case than in the previous one.

* E-mail: yamaguchi@acty.phys.sci.osaka-u.ac.jp

[S1] M. Yamaguchi, K. Kamide, T. Ogawa, and Y. Yamamoto, New J. Phys. **14**, 065001 (2012).

[S2] $T = 10$ K is also different from the previous condition $T = 0$ K but this difference does not play any significant role because $k_{\rm B}T$ is smaller than $\hbar\gamma$.